Journal of Power Sources 210 (2012) 1–6

Contents lists available at SciVerse ScienceDirect

Journal of Power Sources

journal homepage: www.elsevier.com/locate/jpowsour

Short communication

Restricted growth of $LiMnPO_4$ nanoparticles evolved from a precursor seed

Tae-Hee Kim[a], Han-Saem Park[a], Myeong-Hee Lee[a], Sang-Young Lee[b,*], Hyun-Kon Song[a,**]

[a] i-School of Green Energy, UNIST, Ulsan 689-798, Republic of Korea
[b] Department of Chemical Engineering, Kangwon National University, Chuncheon, Kangwon, Republic of Korea

ARTICLE INFO

Article history:
Received 25 January 2012
Received in revised form 14 February 2012
Accepted 15 February 2012
Available online 10 March 2012

Keywords:
Lithium ion batteries
Lithium manganese phosphate
Cathodes
Precipitation
Nanostructure

ABSTRACT

Herein, we report on a novel precipitation method to enable $LiMnPO_4$ olivine (LMP) as a cathode material for lithium ion batteries (LIBs) to reach high capacity at high discharge rates. By confining $Mn_3(PO_4)_2$ precipitation on surface of a precursor seed of Li_3PO_4, the size of LMP particles is limited to less than 100 nm for a smaller dimension. The cathode material delivers discharge capacities of 145 mAh g^{-1} at 0.1 C, 112 mAh g^{-1} at 1 C to 62 mAh g^{-1} at 5 C (comparable with top three performances [1–3]). Even if precipitation is one of the versatile strategies to prepare the cathode material, it has not been reported that such a first-tier high performance is obtained from LMP prepared by precipitation methods. When compared with LMP particles synthesized by a conventional co-precipitation method, the performances are recognized to be considerably enhanced. Also, the surface-confined precipitation process described in this work does not involve a ball milling step with a conductive agent such as carbon black [1,2,4–10] so that a low cost synthesis is feasible.

1. Introduction

Phospho-olivines ($LiMPO_4$ where M = Fe, Mn, Co, Ni) have been considered as one of the most potential cathode materials for LIBs, based on a well-defined two phase reaction coupled with one equivalent electron: $LiMPO_4 \leftrightarrow Li^+ + MPO_4 + e^-$ [1–10]. The strongest reason for interests in the materials is their relatively high theoretical capacity (~170 mAh g^{-1}) compared with that of more traditional cathode materials such as $LiCoO_2$ layered structure (140 mAh g^{-1} within a structurally stable range [11]) and $LiMn_2O_4$ spinel (148 mAh g^{-1} [12]). However, the higher capacity of $LiMPO_4$ does not always lead to higher energy density because energy density results from the product of its working potential as well as its capacity. $LiFePO_4$, the most representative member of the phospho-olivine family, shows its energy density at 585 Wh kg^{-1} that is the value lower than that of $LiMn_2O_4$ spinel (607 Wh kg^{-1}). The main cause of the inferior energy density of $LiFePO_4$ is its low working potential at 3.45 V (versus ~4.1 V for $LiMn_2O_4$). By changing the transition metal constituent of $LiMPO_4$ from Fe to Mn, Co or Ni, its working potential is controlled to be higher values: 4.1 V for M = Mn in $LiMPO_4$, [13]: 4.8 V for Co [14]: and 5.2 V for Ni [15].

In the case of M = Fe in phospho-olivines, we demonstrated that a sequential precipitation in which two different intermediate precipitates (Li_3PO_4 and $M_3(PO_4)_2$) are formed not simultaneously but consecutively leads to a hollow secondary structure consisting of carbon-coated primary particles [16]. The resultant structure was helpful to overcome demerits of $LiFePO_4$ such as low electronic and ionic conductivities: ($\kappa_e = 10^{-9}$ to 10^{-8} S cm^{-1} and $D_i = 10^{-8}$ to 10^{-7} cm^2 s^{-1}, respectively) [12]. In the other members of the phospho-olivine family, the demerits become even more serious with slower electronic transport (κ_e) even if higher energy density is thermodynamically achievable: $\kappa_e = 10^{-11}$ to 10^{-8}, 10^{-11} to 10^{-9} and 10^{-14} to 10^{-11} S cm^{-1} while $D_i = 10^{-9}$ to 10^{-7}, 10^{-9} to 10^{-5} and 10^{-5} cm^2 s^{-1} for M = Mn, Co and Ni in order [6,17,18]. Therefore, the sequential precipitation method with some modification was applied to $LiMnPO_4$ system in this work to get the same advantages (Fig. 1).

2. Experimental

2.1. Preparation

Olivine $LiMnPO_4$ was synthesized by precipitating $Mn_3(PO_4)_2$ on thermally hardened Li_3PO_4 seeds (Fig. 1). The Li_3PO_4 seeds were precipitated by introducing 10 mmol H_3PO_4 to a solution prepared by dissolving 30 mmol LiOH in 12 ml water. The seeds were filtered and then thermally hardened at 300 °C for 3 h. The thermally hardened seeds were re-dispersed in 12 ml water and 10 mmol $MnSO_4$ was added to the re-dispersed solution. The dried mixture of Li_3PO_4 and $Mn_3(PO_4)_2$ was calcined at 600 °C for 10 h in an inert atmosphere. For coating the resultant LMP, sucrose was mixed with LMP in water at 50 wt.% of the active materials followed by drying and heating at 600 °C for 6 h. As a control, LMP was prepared by

* Corresponding author.
** Corresponding author. Tel.: +82 52 217 2512; fax: +82 52 217 2909.
E-mail addresses: syleek@kangwon.ac.kr (S.-Y. Lee), philiphobi@hotmail.com (H.-K. Song).

0378-7753/$ – see front matter © 2012 Elsevier B.V. All rights reserved.
doi:10.1016/j.jpowsour.2012.02.078

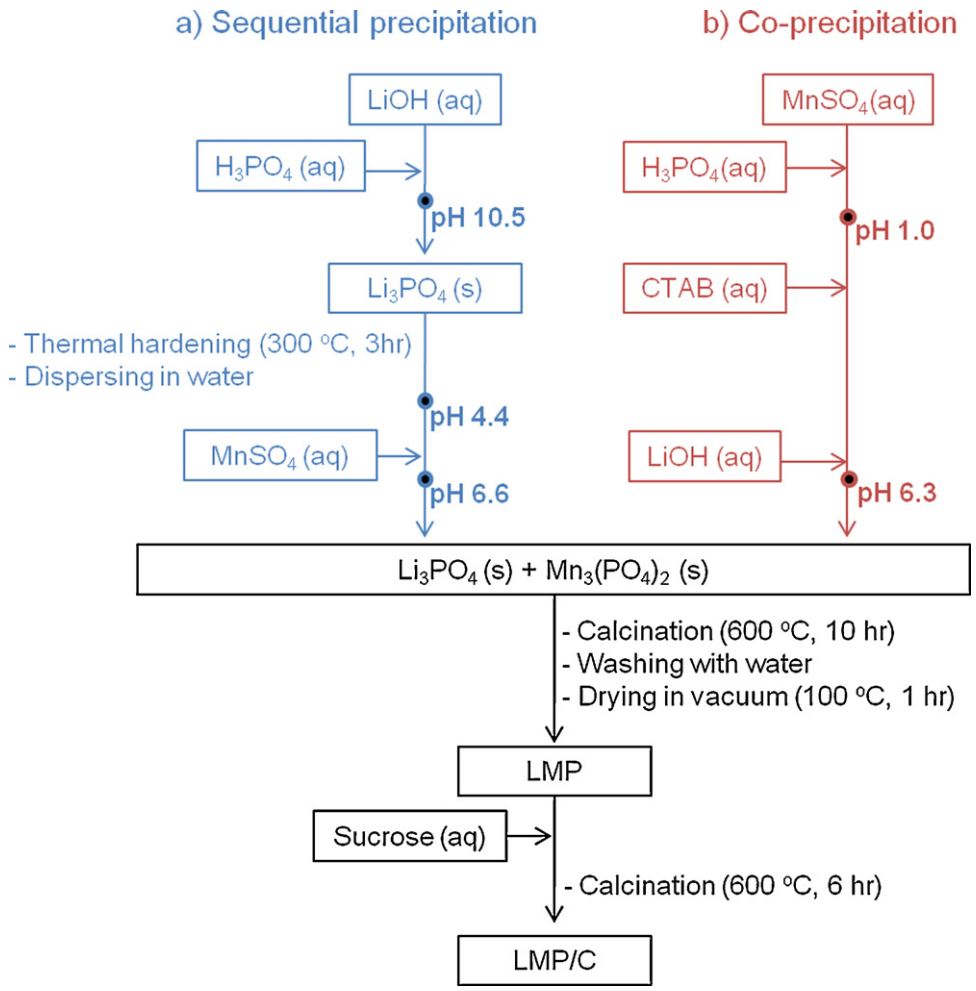

Fig. 1. Synthesis of LMP via two different strategies of precipitation: (a) surface-confined precipitation and (b) co-precipitation.

co-precipitation. The same amounts of precursors were used as those of our surface-confined method described above.

2.2. Cell construction

The 2016R-type coin half cell configuration was used with 1.15 M $LiPF_6$ in 3:7 (v/v) ethylene carbonate/dimethyl carbonate (EC/DMC) as electrolyte for charge and discharge tests. Lithium foil was used as anode. Cathode was constructed by mixing active materials, polyvinylidene fluoride (PVdF) as a binder and Super P carbon black as a conduction enhancer at a weight ratio of 7:1:2 in N-methyl-2-pyrrolidone as a solvent. The mixed slurry was cast onto Al foil by a doctor blade coater; heated at 110 °C for 1 h to evaporate its solvent; and then pressed by using a roll press. The resultant electrodes are specified by densities of the active materials: areal density (d_a) = 2.54 mg cm^{-2}; volumetric density (d_v) = 0.63 g cm^{-3}; thickness = 40 μm.

3. Results and discussion

3.1. Preparation

In the first precipitation step, the first intermediate precipitate Li_3PO_4 is formed with a solubility product K_{sp1} [19]:

$$3Li^+(aq) + PO_4^{3-}(aq) \leftrightarrow Li_3PO_4(s) \quad \text{with} K_{sp1} = [Li^+]^3[PO_4^{3-}] = 2.37 \times 10^{-11} \quad (1)$$

Filtered Li_3PO_4 precipitates were sintered at 300 °C for 3 h for thermal hardening and then re-dispersed in water. Formation of the second precipitate $Mn_3(PO_4)_2$ is followed with the lower value of solubility product K_{sp2} [20]:

$$3Mn^{2+}(aq) + 2PO_4^{3-}(aq) \leftrightarrow Mn_3(PO_4)_2(s) \quad \text{with} K_{sp2} = [Mn^{2+}]^3[PO_4^{3-}]^2 = 1.0 \times 10^{-27} \quad (2)$$

PO_4^{3-} is supplied only by re-solubilization process of pre-formed Li_3PO_4 particles to keep its equilibrium at K_{sp1} so that the formation of $Mn_3(PO_4)_2$ is localized specifically on surface of the Li_3PO_4 particles.

Morphology of precipitates was traced step-by-step by electron microscopes (Fig. 2). The first precipitate Li_3PO_4 was shaped as a hollow sphere (diameter = ~300 nm) by the re-solubilization–precipitation cycles between Li_2HPO_4 and Li_3PO_4 (Fig. 2a–c) [16]. The ~70 nm-thick shell of the hollow spheres consists of primary particles of ~10 nm diameter. The solid sphere in Fig. 2a represents a primary particle of Li_3PO_4 without the exact consideration of dimension: wall of the hollow sphere consists of multiple layers of the primary particles. Precipitation of $Mn_3(PO_4)_2$ on surface of each primary particle of Li_3PO_4 leads to grouping the particles into a fragmented unit, disassembling the hollow secondary structure (Fig. 2d–f). A trace of hollow spheres still observed in insets of Fig. 2e and f confirms that the nanoparticles originate from wall of the hollow structure. During calcination at 600 °C for 6 h, each fragment of mixed precipitates ($Li_3PO_4 + Mn_3(PO_4)_2$) turns into a single LMP particle (Fig. 2g–i).

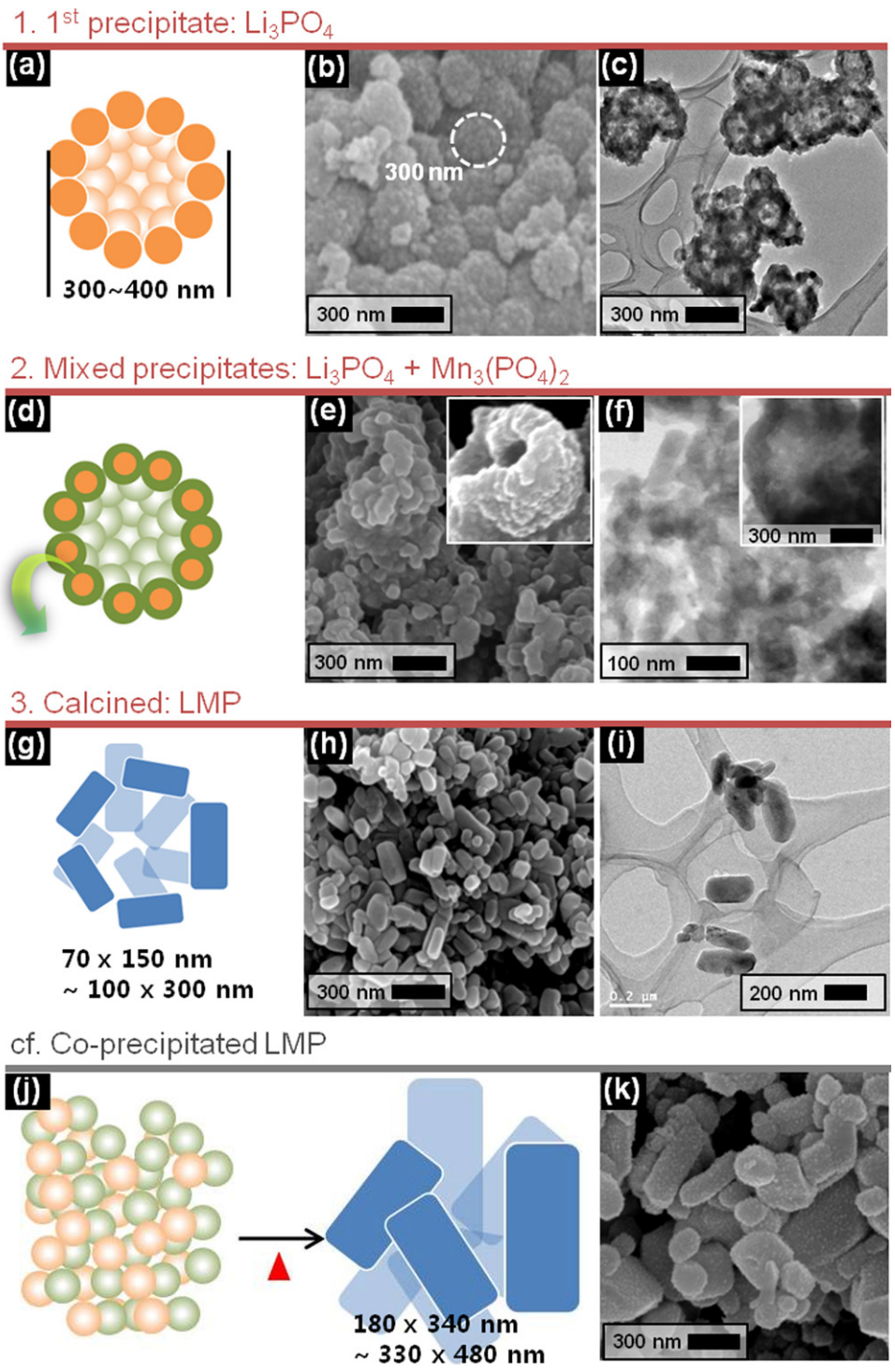

Fig. 2. (a–i) Schematic cartoons and electron microscopy images of LMP particles obtained from each step of the surface-confined precipitation: (a–c) the first precipitates (Li_3PO_4); (d–f) the mixture of the first (orange) and the second (green) precipitates obtained after the second precipitation; (g–i) the sample obtained after calcination. (j–k) Schematic cartoons and electron microscopy images of co-precipitated LMP as a control for comparison. (For interpretation of the references to color in this figure legend, the reader is referred to the web version of the article.)

The size-restriction effect of the surface-confined precipitation can be clearly emphasized when the electron-micrographic images are compared between our method and co-precipitation (Fig. 2j and k): 70 nm × 150 nm–100 nm × 300 nm for our surface-confined precipitation versus 180 nm × 340 nm–330 nm × 480 nm for co-precipitation. The effect of size reduction of LMP particles on battery performances is predicted positive by surveying trends of capacity versus particle size with comprehensive data collected from literatures (Fig. S2a with Table S1 in Supporting information).

When compared with M = Fe in $LiMPO_4$ ($K_{sp} = 1.0 \times 10^{-36}$), the hollow secondary structure of Li_3PO_4 was not maintained in the case of M = Mn. The structural difference is believed to come from the difference of K_{sp}. As presumed from its higher value of K_{sp}, $Mn_3(PO_4)_2$ is more difficult to precipitate or requires more amount

of free PO_4^{3-} in aqueous phase for precipitation. Therefore, more amount of Li_3PO_4 is required to be dissolved for initiating the second precipitation when Mn^{2+} ion is introduced to the suspension of Li_3PO_4 made via the first precipitation step. More abundant loss of mass before the second precipitation leads to weakening a structural prop of the hollow secondary structure.

The crystallographic structure by X-ray diffraction (XRD) and the chemical composition by inductively coupled plasma atomic emission spectroscopy (ICP-AES) proved the successful synthesis of LMP olivine, however, with Li_3PO_4 as a minor impurity phase (Fig. 3). The molar composition of LMP was estimated at Li:Mn:P = 1.2:0.96:1.0 by ICP-AES. From the stoichiometric calculation with an assumption of the mixture consisting of $LiMnPO_4 + xLi_3PO_4$, ~6.5 molar%, equivalent to ~5 wt.% Li_3PO_4, was detected. The minor phase can be easily removed by weak acid such as diluted acetic or phosphoric acid. The products from each step of the surface-confined precipitation were also identified by XRD. There was no difference between before and after thermal hardening process, XRD showing well-defined crystalline Li_3PO_4. After the second precipitation, unknown peaks that would be assigned to the second precipitate Mn_3PO_4 appeared in addition to the spectra of previous step.

Due to its low electronic conductivity, surface-coating with a conductive material is required for LMP like the case of its sister

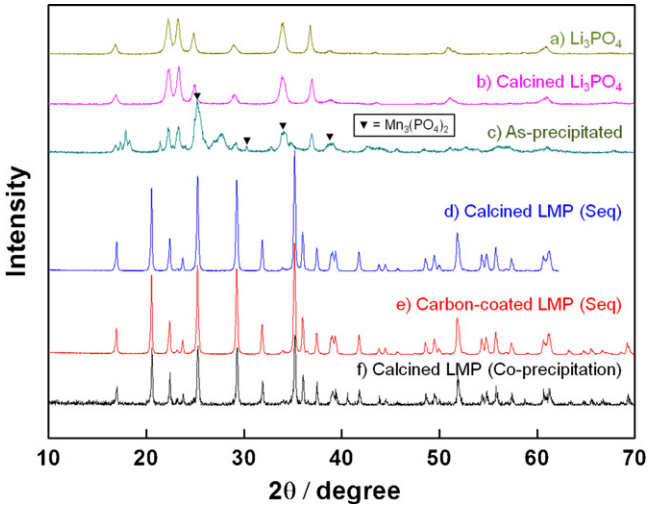

Fig. 3. X-ray diffraction patterns of the first intermediate precipitate (Li_3PO_4, a and b), the mixed intermediate precipitate ($Li_3PO_4 + Mn_3(PO_4)_2$, c), the thermally treated one ($LiMnPO_4$, d) and carbon-coated one ($LiMnPO_4$, d) obtained through each step of the surface-confined precipitation. For a comparison, the co-precipitated LMP is shown (f).

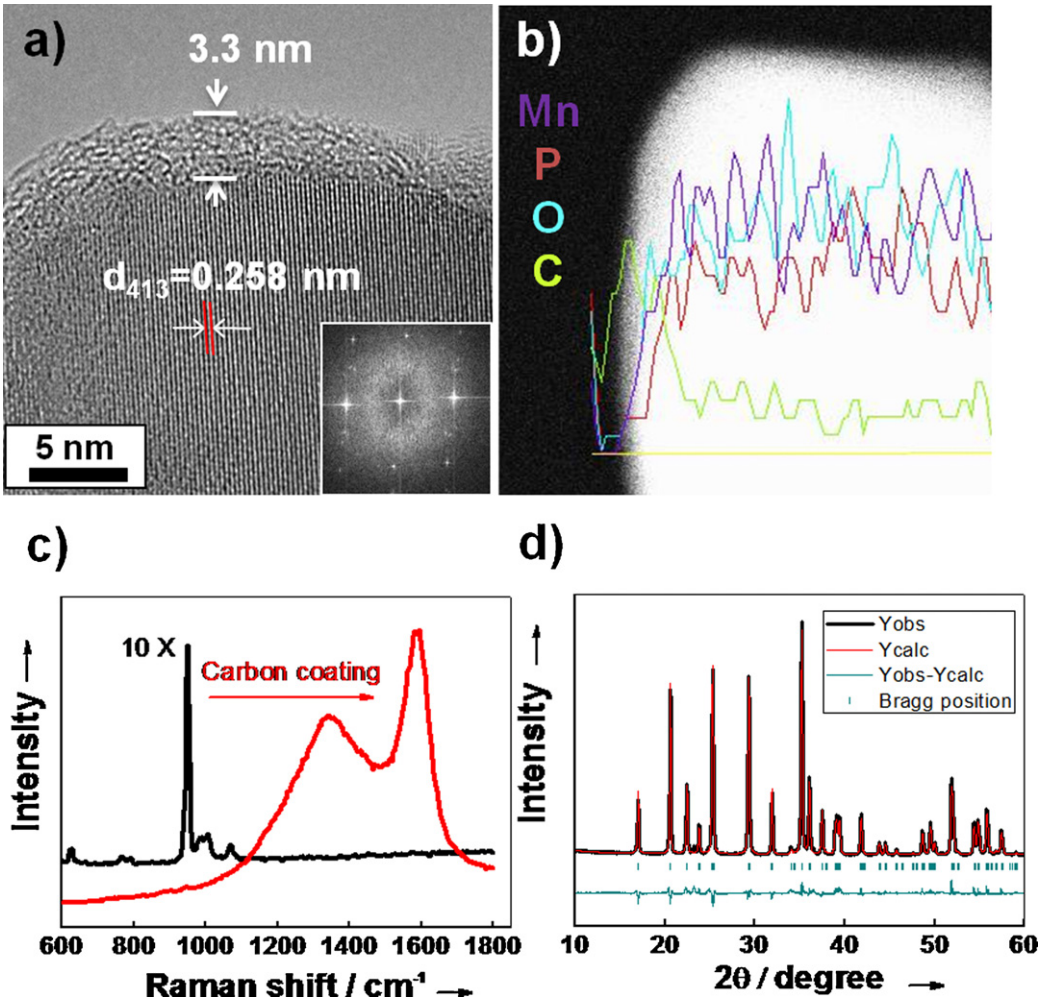

Fig. 4. (a) A representative transmission-electron-microscopic (TEM) image of a single carbon-coated LMP particle with its Fourier-transformed pattern as an inset. (b) A line mapping of the constituents of a single carbon-coated LMP particle in the same scale of (a). (c) Raman spectra of bare LMP (black, intensity-magnified by 10×) and carbon-coated LMP (red). (d) X-ray diffraction (XRD) pattern of carbon-coated LMP. There was no significant difference between bare and carbon-coated LMPs in terms of the XRD pattern. (For interpretation of the references to color in this figure legend, the reader is referred to the web version of the article.)

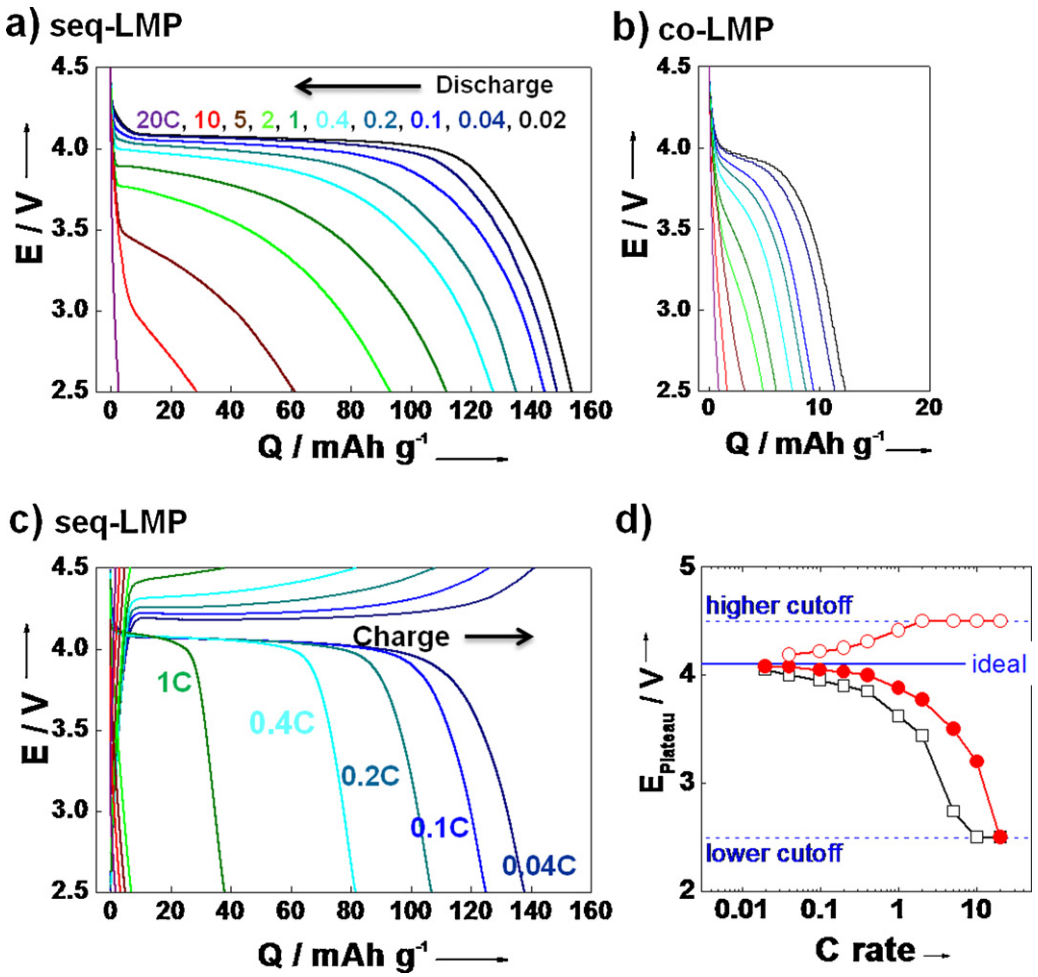

Fig. 5. (a–c) Potential profiles of half coin cells of sequentially precipitated LMP (seq-LMP, a and c) and co-precipitated LMP (co-LMP, b). 1.0 C = 150 mAh g^{-1}. The cells in a and b were charged at 0.04 C up to 4.5 V followed by keeping the potential until current flowed below a hundredth of the charging current. Then they were discharged at various C rates as indicated. The cells in c were charged at various C rates of constant current as indicated (not followed by keeping them at constant voltage). Then they were discharged at 0.04 C immediately after being charged. (d) C-rate dependency of plateau potential ($E_{plateau}$) during discharge or charge. Red solid circle, seq-LMP during discharge; red open circle, seq-LMP during charge; black open square, co-LMP during discharge. (For interpretation of the references to color in this figure legend, the reader is referred to the web version of the article.)

compound $LiFePO_4$. Carbon as a conductive material is well known to play a crucial role for enhancing performances of cathode materials for LIBs. Higher carbon contents in a coating and/or an electrode composite are expected to result in less loss of energy by facilitating electron flow between current collectors and active materials. Even if cell capacity is roughly proportional to carbon contents (resulting from literature survey, Fig. S2b in Supporting information), the details of carbons would be more important: graphitic degree, percolation extent, ratio between coating and bulk and so on. An in situ carbon-coating where a carbon precursor is assembled into a composite with active material during synthesis (here, precipitation) was tried but failed. The same technique was used in our previous work for $LiFePO_4$ with CTAB (cetyltrimethylammonium bromide) as a carbon precursor [16]. In this work, good quality of carbon coating (2–4 wt. %) wrapping primary particles was successfully obtained even if CTAB is completely decomposed to a zero mass at <300 °C much lower than calcination temperature of the $LiFePO_4$ (endothermic peak at 260 °C under an inert atmosphere in thermogravimetric analysis (TGA), preliminary data). On the contrary, there was very little (0.04–0.08 wt.% within error range of analysis) or no carbon contents remaining for LMP with CTAB as a carbon precursor after calcination. We believe that this difference of degree of CTAB carbonization comes from the difference of metals (M in $LiMPO_4$). When considering that Fe, Ni, Cr, Al and Cu are generally recognized as catalysts for carbonization [21,22], not Mn but Fe is considered to make some helpful catalytic effects on carbonization. This interpretation can be supported by the fact that a considerable amount of carbon (~1.5 wt.%) was obtained with Li $Mn_{0.5}Fe_{0.5}PO_4$ from CTAB in our preliminary experiments.

Instead of the in situ carbon coating, therefore, LMP was coated with carbon in a widely used post-synthetic way of sucrose coating followed by calcination. Nanoparticles were successfully coated homogeneously with 8.5 wt.% carbon (assayed by a combustion method), which is clearly shown by TEM and a line mapping of carbon element (Fig. 4a and b). By carbon coating, in Raman spectra, phosphate-related peak at 950 cm^{-1} turned unclear with two high-intensity peaks assigned to carbon's D and G bands at 1345 cm^{-1} and 1590 cm^{-1} (Fig. 4c). No significant crystallographic difference was observed between bare and carbon-coated LMP (Figs. 3 and 4d). The Rietveld-refined lattice parameters based on the orthorhombic Pmnb matched closely to the values from a crystallographic database (JCPDS No. 33-0804): bare and carbon-coated LMPs versus

database, a (Å) = 6.1030 and 6.0988 versus 6.1000; b (Å) = 10.4406 and 10.4385 versus 10.4600; c (Å) = 4.7462 and 4.7415 versus 4.7440.

3.2. Electrochemical performances

The LMP prepared by the surface-confined precipitation (seq-LMP) was tested as a cathodic material for LIBs. In spite of its poor conductivities, the LMP showed good discharge performance from 153 mAh g^{-1} at 0.02 C to 62 mAh g^{-1} at 5 C (Fig. 5a). However, it was difficult at >10 C to find a flat potential behavior based on faradaic reaction of LMP because operational current exceeds the kinetics of lithiation of $MnPO_4$ during discharge process. When compared with co-precipitated LMP (co-LMP, Fig. 5b), the improvement of discharge capacities of seq-LMP would be emphasized. The distinguishingly superior capacities of seq-LMP over co-LMP are ascribed to its smaller particle size: $d_{seq} = \sim 1/3 d_{co}$ (70–100 nm for seq-LMP versus 180–330 nm for co-LMP) where d = a characteristic dimension of LMP particles. The particle size affects primarily ionic conductance (as an extensive property, not conductivity) and also indirectly electronic conductance. With the same amount of carbon for coating, smaller particles lead to higher degree of percolation of conductive network. The conductance of seq-LMP-based electrodes would be about ten ($=3^2$) times as high as that of co-LMP electrodes if the following assumption is applicable: electric conductance from current collector to a LMP particle $\propto$ connectivity of the LMP particle to a conductive phase $\propto$ surface area of the LMP particle. In addition to discharge capacity, deviation of plateau potential ($E_{plateau}$) from ideal value (4.1 V) in voltage profiles is a measure of goodness of charge transport. The gap of $E_{plateau}$ between seq-LMP and co-LMP widens as the discharge rate increases, proving better properties of seq-LMP (Fig. 5d).

In addition to discharge properties, charge characteristics were also investigated (Fig. 5c). Even if high working potential of LMP (versus $LiFePO_4$) provides an advantage in terms of energy density for discharge, the narrower potential margin from the working potential (ideally 4.1 V) to the cut-off potential (4.5 V) leads to a demerit of incomplete charge at fast rates (without keeping voltage at the cut-off potential). The asymmetric potential margin is the main reason why charge capacity is much less than discharge capacity even at the same rate even if asymmetric kinetics of LMP might be partly responsible: for example, 128 mAh g^{-1} for discharge versus 82 mAh g^{-1} for charge at 0.4 C.

4. Conclusions

In this work, we proposed the method to restrict the growth of particle size of LMP during precipitation (called surface-confined precipitation from the viewpoint of synthetic mechanism or sequential precipitation from the viewpoint of synthetic method). The size-limited nanoparticles of <100 nm in a shorter dimension delivered good performances at fairly high rates when compared with a co-precipitated counterpart. This surface-confined precipitation method provides a cost-effective strategy for synthesizing high performance LMP, not including ball milling processes for pulverizing particles and mixing with carbon particles but enabling a continuous synthetic process.

Acknowledgments

This work was supported by the Ministry of Education, Science and Technology (WCU:R31-2008-000-20012-0 and CRC: 2011K000637) and the Ministry of Knowledge Economy (R0000491 and NIPA-2011-C1090-1100-0002), Korea.

Appendix A. Supplementary data

Supplementary data associated with this article can be found, in the online version, at doi:10.1016/j.jpowsour.2012.02.078.

References

[1] D.W. Choi, D.H. Wang, I.T. Bae, J. Xiao, Z.M. Nie, W. Wang, V.V. Viswanathan, Y.J. Lee, J.G. Zhang, G.L. Graff, Z.G. Yang, J. Liu, Nano Lett. 10 (2010) 2799–2805.
[2] S.M. Oh, S.W. Oh, C.S. Yoon, B. Scrosati, K. Amine, Y.K. Sun, Adv. Funct. Mater. 20 (2010) 3260–3265.
[3] H. Yoo, M. Jo, B.S. Jin, H.S. Kim, J. Cho, Adv. Energy Mater. 1 (2011) 347–351.
[4] G.H. Li, H. Azuma, M. Tohda, Electrochem. Solid-State Lett. 5 (2002) A135–A137.
[5] C. Delacourt, P. Poizot, M. Morcrette, J.M. Tarascon, C. Masquelier, Chem. Mater. 16 (2004) 93–99.
[6] C. Delacourt, L. Laffont, R. Bouchet, C. Wurm, J.B. Leriche, M. Morcrette, J.M. Tarascon, C. Masquelier, J. Electrochem. Soc. 152 (2005) A913–A921.
[7] N.N. Bramnik, H. Ehrenberg, J. Alloys Compd. 464 (2008) 259–264.
[8] S.K. Martha, J. Grinblat, O. Haik, E. Zinigrad, T. Drezen, J.H. Miners, I. Exnar, A. Kay, B. Markovsky, D. Aurbach, Angew. Chem. Int. Ed. 48 (2009) 8559–8563.
[9] S.K. Martha, B. Markovsky, J. Grinblat, Y. Gofer, O. Haik, E. Zinigrad, D. Aurbach, T. Drezen, D. Wang, G. Deghenghi, I. Exnar, J. Electrochem. Soc. 156 (2009) A541–A552.
[10] D.Y. Wang, H. Buqa, M. Crouzet, G. Deghenghi, T. Drezen, I. Exnar, N.H. Kwon, J.H. Miners, L. Poletto, M. Graetzel, J. Power Sources 189 (2009) 624–628.
[11] S.A. Needham, G.X. Wang, H.K. Liu, V.A. Drozd, R.S. Liu, J. Power Sources 174 (2007) 828–831.
[12] O.K. Park, Y. Cho, S. Lee, H.C. Yoo, H.K. Song, J. Cho, Energy Environ. Sci. 4 (2011) 1621–1633.
[13] A.K. Padhi, K.S. Nanjundaswamy, J.B. Goodenough, J. Electrochem. Soc. 144 (1997) 1188–1194.
[14] K. Amine, H. Yasuda, M. Yamachi, Electrochem. Solid-State Lett. 3 (2000) 178–179.
[15] J. Wolfenstine, J. Allen, J. Power Sources 142 (2005) 389–390.
[16] M.H. Lee, J.Y. Kim, H.K. Song, Chem. Commun. 46 (2010) 6795–6797.
[17] K. Rissouli, K. Benkhouja, J.R. Ramos-Barrado, C. Julien, Mater. Sci. Eng. B-Solid 98 (2003) 185–189.
[18] D. Morgan, A. Van der Ven, G. Ceder, Electrochem. Solid-State Lett. 7 (2004) A30–A32.
[19] J.A. Dean, Lange's Handbook of Chemistry, 13th ed., McGraw-Hill, New York, 1985.
[20] F.W. Boyle, W.L. Lindsay, Soil Sci. Soc. Am. J. 49 (1985) 761–766.
[21] F.J. Maldonado-Hodar, C. Moreno-Castilla, J. Rivera-Utrilla, Y. Hanzawa, Y. Yamada, Langmuir 16 (2000) 4367–4373.
[22] C.J. Lee, J. Park, J.A. Yu, Chem. Phys. Lett. 360 (2002) 250–255.